

## Direct Visualization of Aggregate Morphology and Dynamics in a Model Soil Organic–Mineral System

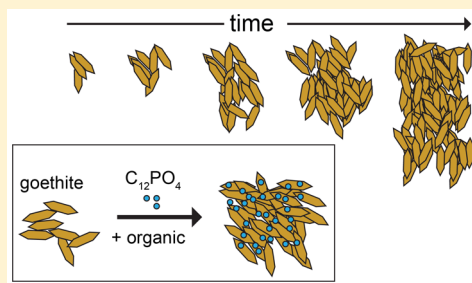
Ryan Hufschmid,<sup>†</sup> Christina J. Newcomb,<sup>‡</sup> Jay W. Grate,<sup>†</sup> James J. De Yoreo,<sup>†,‡</sup> Nigel D. Browning,<sup>†,‡</sup> and Nikolla P. Qafoku<sup>\*,‡</sup>

<sup>†</sup>Department of Materials Science and Engineering, University of Washington, Seattle, Washington 98195-2120, United States

<sup>‡</sup>Pacific Northwest National Laboratory, Richland, Washington 99352, United States

### Supporting Information

**ABSTRACT:** Interactions between mineral surfaces and organic matter are ubiquitous in soils and the environment. Through both physical and chemical mechanisms, organic–mineral assemblages prevent decomposition of soil organic matter by limiting accessibility or reducing efficacy of enzymes and microbes. To understand the mechanisms underlying organic–mineral interactions, researchers have begun to interrogate these systems at micro- and nanometer length scales. Current techniques that maintain a hydrated state and allow researchers to characterize nanometer length scales are limited. Here we chose a model organic–mineral system and performed complementary imaging techniques that allowed direct nanoscale observations in environmentally relevant conditions: cryogenic transmission electron microscopy (cryo-TEM) and *in situ* liquid cell transmission electron microscopy (TEM). We observed a 3-fold increase in the aggregate size of goethite nanoparticles upon addition of a model organic phosphate ligand and a preference for side-to-side interactions independent of the addition of the organic ligand. Additionally, *in situ* liquid cell TEM experiments provided a dynamic view of the interactions allowing us to report velocities of mineral assemblages during aggregation and disaggregation, which could potentially provide binding energetics and kinetic parameters for organic–mineral and mineral–mineral systems.



### INTRODUCTION

Soil aggregates are the building blocks of soil and are held together primarily through organo–mineral associations.<sup>1,2</sup> It is well accepted that the organic species that “glue” the mineral particles together are highly persistent and reside in soils for long periods of time.<sup>3</sup> The degree to which minerals aggregate in soils depends on the interactive chemistry between mineral surfaces and organic molecules and local environmental conditions such as hydrology, pH, and ionic strength. Characterizing the early steps in aggregate formation may allow researchers to predict how the aggregate-associated carbon is stabilized and determine under which conditions this carbon pool can become more mobile.

Microbes and soil organic matter are mobilized by water films; therefore, to understand the dynamics involved during aggregation, visualizing nanoscale interactions in a hydrated environment is of particular interest.<sup>4</sup> Techniques that are commonly used by soil and geosciences include attenuated total reflectance Fourier transform infrared spectroscopy (ATR-FTIR), scanning transmission X-ray microscopy (STXM), and nano-secondary ion mass spectrometry (NanoSIMS). While ATR-FTIR allows researchers to monitor hydrated molecular signatures at the organic–mineral interface, monitoring the morphology of nanoscale aggregation is not possible. To characterize these interactions, STXM, near edge X-ray absorption fine structure (NEXAFS), and NanoSIMS are powerful techniques for locating and identifying the chemistry

of molecules at a resolution of tens of nanometers; however, measurements under aqueous conditions are challenging,<sup>5</sup> often resulting in a static interpretation of the system.

Recent advances in electron microscopy provide researchers with new approaches for probing interactions at the nanoscale. Cryogenic transmission electron microscopy (cryo-TEM) allows visualization of nanoscale structures through a thin vitreous layer of solvent, which maintains the hydrated state of the sample. *In situ* liquid electron microscopy allows nanoscale specimens to be imaged during a reaction under relevant environmental conditions.<sup>6,7</sup> Solutions are encapsulated between chips with electron-transparent membranes using specialized specimen holders. In this way, dynamics of liquid phase systems can be observed without compromising the high vacuum of the transmission electron microscope.<sup>8</sup> This approach has been used to study nucleation and growth,<sup>9,10</sup> oriented attachment,<sup>11,12</sup> and electrochemistry.<sup>13</sup> The experiments can be complex to design, perform, and interpret; however, cryo-TEM can provide complementary information with similar samples and is capable of producing higher-resolution images.

Received: February 28, 2017

Revised: March 30, 2017

Accepted: March 30, 2017

Published: March 30, 2017

Here we leverage the advantages of both complementary techniques, *in situ* TEM and cryo-TEM.<sup>4</sup> Using a mechanistic approach to probe the complex process of aggregation, we implement these imaging modalities to monitor the aggregation behavior of a model organic–mineral system under hydrated, environmentally relevant conditions. Based on their size, the soil aggregates are classified as follows: domains or assemblages ( $< 2 \mu\text{m}$ ), clusters ( $2\text{--}20 \mu\text{m}$ ), microaggregates ( $20\text{--}250 \mu\text{m}$ ), and macroaggregates ( $250\text{--}2000 \mu\text{m}$ ). By evaluating the morphology of organic–mineral complexes at the nanoscale, we can visualize how organic ligands influence the behavior of minerals. Additionally, *in situ* liquid cell TEM provides a dynamic view of organic–mineral interactions at the nanoscale.

## MATERIALS AND METHODS

**Materials and Preparation.** All chemicals used in this work were used as received and purchased from Sigma-Aldrich unless otherwise noted.

Goethite was synthesized as described previously.<sup>14</sup> Briefly, a 0.5 M Fe(III) nitrate solution was slowly neutralized with 2.5 M NaOH until the pH of the solution reached 12. This mixture was aged in an oven at  $60 \text{ }^\circ\text{C}$  for 90–110 h and dialyzed against water for 2 weeks until the resistivity of the solution was constant. BET measurements (using nitrogen as the adsorbate) revealed a surface area of  $94.9 \text{ g/cm}^2$ . The nanoparticles were kept in a water suspension until they were used at pH 4, which is lower than the point of zero charge to minimize aggregation prior to experiments. For experiments, the pH of the goethite was then adjusted to 6 and the solution diluted to the desired concentration in 10 mM NaCl.

The sodium dodecyl phosphoric acid ( $\text{C}_{12}\text{PO}_4$ ) was used as received. For experiments,  $\text{C}_{12}\text{PO}_4$  was dissolved at a concentration of 10 mM, filtered through a  $0.2 \mu\text{m}$  filter, and diluted to 0.1 mM prior to experiments. In experiments that combined both goethite and organic ligand, equal volumes of each were added in 10 mM NaCl at pH 6.

**Conventional and Cryogenic TEM.** Conventional TEM was performed on an FEI Tecnai TEM instrument operating at 200 kV. Images were collected using an FEI Eagle camera. Samples were drop cast on 300 mesh copper grids with carbon support. The  $\text{C}_{12}\text{PO}_4$  sample was negatively stained using a 2% phosphotungstic acid solution.

Cryo-TEM samples were prepared and allowed to incubate for approximately 30 min prior to preparation using an FEI Vitrobot Mark III (FEI, Hillsboro, OR). The goethite only sample was imaged at 0.1 mg/mL in 10 mM NaCl at pH 6, while mixtures with final concentrations of 0.1 mg/mL goethite and 0.1 mM  $\text{C}_{12}\text{PO}_4$  were imaged in 10 mM NaCl at pH 6. For sample preparation, briefly,  $4 \mu\text{L}$  of the sample was deposited on a 300 mesh copper TEM grid with a lacey carbon support film (Electron Microscopy Sciences, Hatfield, PA). Samples were maintained at a minimum of 70% humidity, plunged into liquid ethane, and transferred under liquid nitrogen to the microscope using a Gatan 626 cryogenic holder. The sample was maintained at  $-175 \text{ }^\circ\text{C}$  or below during transfer and while imaging using an FEI Tecnai TEM instrument equipped with a LaB<sub>6</sub> filament operating at an accelerating voltage of 120 kV. Images were collected using a Gatan  $2 \times 2\text{K}$  Ultrascan 1000 CCD camera and Gatan Digital Micrograph software.

**In Situ TEM.** *In situ* (scanning) (S)TEM was performed on a C<sub>s</sub>-corrected FEI Titan instrument operated at 300 kV. The electron dose rate was determined from the calibrated probe current, as previously described.<sup>15,16</sup> Liquid TEM was

performed on a Hummingbird Scientific liquid stage, with a closed cell (no flow) and 50 nm thick silicon nitride membranes. Liquid cells were prepared by combining  $0.2 \mu\text{L}$  of a 0.1 mg/mL goethite suspension with  $0.2 \mu\text{L}$  of 0.1 mM  $\text{C}_{12}\text{PO}_4$  (all solutions were in 10 mM NaCl). Approximately 30 min passed between mixing of the solutions and TEM imaging. This was the time required to assemble the liquid cells, insert the holder, and allow vacuum to reach appropriate levels, so 30 min was used in all experiments.

**Dynamic Light Scattering.** Dynamic light scattering (DLS) was performed using a Horiba SZ-100 nanoparticle analyzer. Solutions of the mineral, the organic, and the combination of the mineral and organic were analyzed at the same concentrations used in TEM experiments. Each sample was measured five times and averaged to provide a final number-average value for the hydrodynamic radius, reported in Table S1.

**Image Analysis.** Cryo-TEM images were analyzed using ImageJ.<sup>17</sup> The size and density of each assemblage and the angle between individual mineral grains were measured. *In situ* assemblage velocities were measured using Tracker (<http://physlets.org/tracker/>), an open source video analysis tool. Details of the image processing and analysis can be found in Figures S1 and S2.

**Statistical Analysis.** Statistical analysis was performed using Graphpad Prism. Each parameter that was quantified by cryo-TEM (area, major axis, minor axis, and angle between crystals) was analyzed by comparing conditions with and without organic added. A two-tailed nonparametric unpaired *t* test (Mann–Whitney test) was performed, and *p* values of  $< 0.001$  were considered significant. To summarize, the area ( $p < 0.0001$ ), major axis ( $p < 0.0001$ ), and minor axis ( $p < 0.0001$ ) were found to be significant and angle measurements were not significant.

## RESULTS AND DISCUSSION

First, we chose a model organic–mineral system to perform cryo-TEM and *in situ* liquid TEM. To understand how aggregates can stabilize soil organic matter, knowledge about the organo–mineral interface is necessary. We chose our model on the basis of the recent conceptual model that describes the interface as having distinct “zones” of interactions.<sup>18</sup> The initial contact zone involves direct bonding of organic molecules to the mineral surface while directly above this surface a “membrane-like bilayer” forms. This hydrophobic zone supports organic–organic interactions shielding hydrophobic moieties from aqueous solvents. Farthest from the mineral surface, a kinetic zone contains molecules that are mobile and interact depending on local environmental conditions. Electron microscopy is well-suited to imaging minerals at this length scale; however, imaging organic matter and other light elements is challenging. Without imaging the mineral–organic interface directly, we will find it difficult to corroborate this zonal model and must infer the behavior of the organic from mineral transformations. With this in mind, we chose monododecyl-phosphate ( $\text{C}_{12}\text{PO}_4$ ) as a model ligand and goethite as a mineral.  $\text{C}_{12}\text{PO}_4$  was chosen as an organic ligand because it is capable of interacting directly at the mineral surface via a phosphate group<sup>19</sup> and can participate in hydrophobic organic–organic interactions through the alkyl tail. Additionally, organic phosphorus constitutes 20–80% of the upper soil horizons<sup>20</sup> and often occurs in nature as esters, which are converted to inorganic phosphorus and taken up by plants. Iron

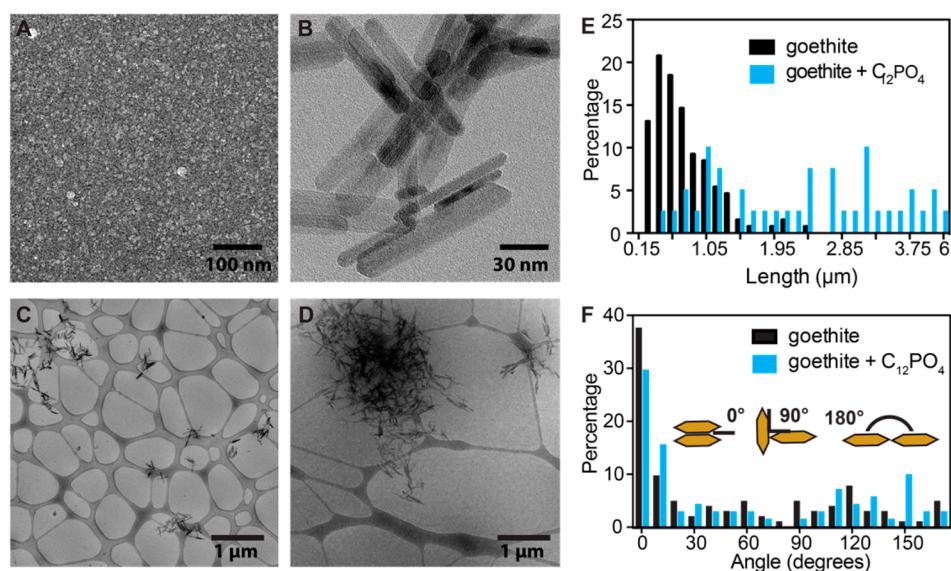


**Figure 1.** Characterization of the model system to interrogate mineral–organic interactions. (A) Conventional TEM images of the model organic ligand,  $C_{12}PO_4$ , filtered from a 10 mg/mL solution in water that was dried and negatively stained for imaging. (B) Conventional TEM of the model goethite nanoparticles dried from a 0.01 mg/mL suspension, unstained. Cryogenic TEM of (C) a suspension of goethite nanoparticles at 0.1 mg/mL in 10 mM NaCl at pH 6, and (D) a suspension of goethite and  $C_{12}PO_4$  in 10 mM NaCl 30 min after mixing (final concentrations of 0.1 mg/mL goethite and 0.1 mM  $C_{12}PO_4$ ). Quantification of the cryogenic TEM images both before and after the addition of the organic ligand shows the effect on (E) the assemblage size (represented as the long axis of each assemblage) of goethite ( $n = 130$ ) and goethite with  $C_{12}PO_4$  ( $n = 40$ ) and (F) the orientation of individual mineral particles (for goethite only,  $n = 71$ ; for goethite with  $C_{12}PO_4$ ,  $n = 104$ ).

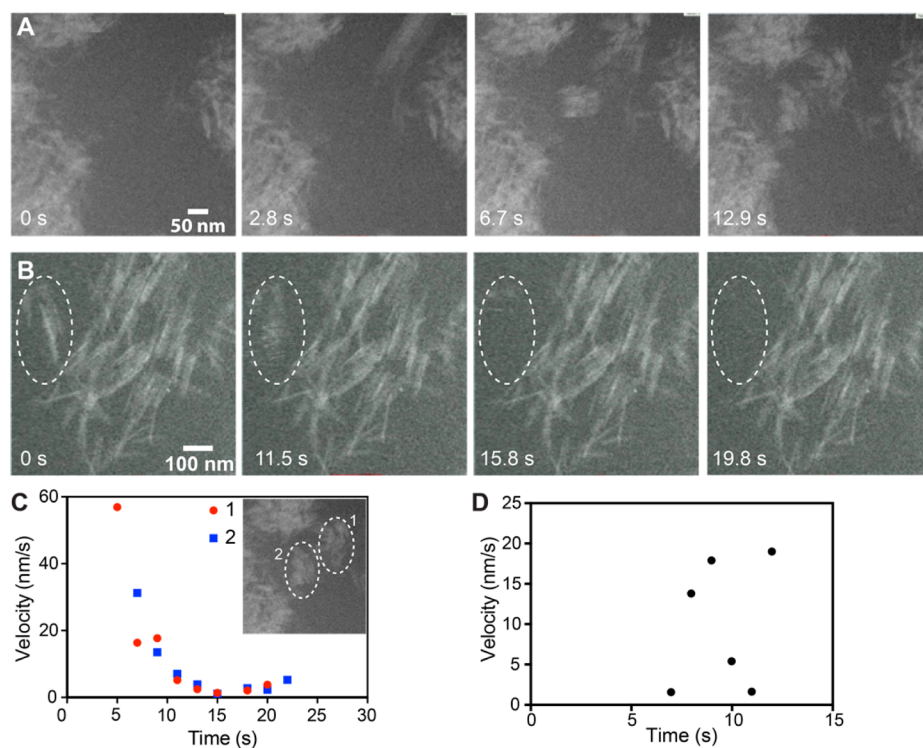


**Figure 2.** *In situ* STEM monitoring of the dynamics of goethite nanoparticles in real time. (A) Time series demonstrating aggregation with particles interacting with existing assemblages. Images were acquired with an electron dose rate of  $1.2 \text{ e}^- \text{ \AA}^{-2} \text{ s}^{-1}$ . (B) Time series demonstrating disaggregation with particles leaving the region of interest (dotted oval). Images were acquired with an electron dose rate of  $0.9 \text{ e}^- \text{ \AA}^{-2} \text{ s}^{-1}$ . (C) Velocities of two different assemblages (outlined with dotted ovals, inset) approaching existing mineral clusters in the field of view from the snapshots shown in panel A. (D) Velocities of an assemblage leaving the field of view (dotted oval from panel B). See the [Supporting Information](#) for the movies.

oxides such as goethite are ubiquitous in soils. Biologically derived phosphates such as phospholipids have been shown to bind strongly to iron oxides through an Fe–O–P complex.<sup>21,22</sup>

Additionally, surface complexes at the organic phosphate–goethite interface have been previously characterized in detail by FTIR.<sup>23</sup>

Next, we imaged both the organic and inorganic components of the system using conventional TEM. Goethite nanoparticles were rod-shaped (Figure 1B), and the organic ligand  $C_{12}PO_4$  self-assembled in aqueous environments to form spherical micelles at the concentrations used (Figure 1A), suggesting that the ligand could provide multivalent interactions with the goethite surface.

To visualize the behavior of the structures under solvated conditions, we then performed cryo-TEM to obtain a snapshot of the interactions in time. The model system was imaged in 10 mM NaCl, a representative ionic strength for soils.<sup>24</sup> The mineral phase was imaged both alone and combined with  $C_{12}PO_4$  30 min after mixing. Qualitatively, we observe that goethite arranges into branching structures (Figure 1C,D). Visualizing the organic ligand was difficult because of a lack of contrast in the presence of the high-contrast mineral. However, the presence of the organic molecule created observable differences in the aggregation of the mineral phase (Figure 1E). The average assemblage size was determined by measuring the major axis of each assemblage in solution. The addition of the organic ligand  $C_{12}PO_4$  increased the average size of the mineral clusters by 230% [aqueous goethite,  $0.68 \pm 0.40 \mu\text{m}$  (mean  $\pm$  standard deviation); goethite with ligand,  $2.25 \pm 1.19 \mu\text{m}$ ]. The standard deviation both with and without the organic is large such that there is some overlap in distributions; however, there is clearly a significant ( $p < 0.0001$ ) increase in cluster size. This difference in assemblage size with the addition of organic molecules is also supported by DLS data, where the hydrodynamic radius increased when both organic and mineral components were mixed (Table S1). The analysis of DLS data relies on the diffusion coefficient that assumes a spherical geometry; because our structures are nonspherical, the relationship between the dimension of the particle and the diffusion coefficient may be poorly represented.<sup>25</sup> Therefore, the DLS data represent a rough measurement for size, and TEM measurements are more direct in nature.

To investigate if goethite exhibited a preferred orientation within the assemblage, the angles between adjacent individual crystal grains were measured. The attachment angle here is defined as the angle between adjacent grains within the assemblages, with  $0^\circ$  being the side-to-side angle and  $180^\circ$  being the end-to-end angle (Figure 1F, inset). The goethite crystals tended to adopt a side-to-side orientation with adjacent grains, as indicated by a large fraction of low-angle ( $<10^\circ$ ) orientations (Figure 1F). There was no significant difference in attachment angle with or without  $C_{12}PO_4$ .

Cryo-TEM captures snapshots of mineral assemblages at specific points in time; however, to monitor the evolution of a specific structure, the dynamics of a single assemblage in real time can be observed using *in situ* liquid phase STEM. Images were acquired using an annular detector, which provided a contrast proportional to the atomic number (Z-contrast). High-contrast, iron-containing minerals appeared bright compared to the dark background containing water, organics, and other light elements. *In situ* liquid STEM of goethite assemblages revealed a branched structure similar to those observed via cryo-TEM. Particles in solution were already interacting prior to the start of the *in situ* experiments. Most of the individual assemblages exhibited little to no observable motion during the experiment, suggesting that the assemblages were relatively stable over the course of 1 h.

Occasionally, aggregation and disaggregation events were observed (panels A and B of Figure 2, respectively). Velocities

are reported for particles throughout the movies and in panels C and D of Figure 2. In panels A and C of Figure 2 (Supplementary Movie 1), assemblages diffuse into the viewing area quickly: particle 1 moving at 52 nm/s and particle 2 moving at 31 nm/s between the first frames. As they approached the surface, the particles rapidly decelerated at a rate of approximately  $1 \text{ nm/s}^2$  for  $\sim 10$  s before coming to rest making contact with the larger assemblage where they remained stable for the remainder of the experiment. The particles' deceleration and the assemblage stability made it convenient to track particle velocity after the first few frames of this aggregation event. A dissociation event is shown in Figure 2B (Supplementary Movie 2). In this movie, the mineral assemblies were relatively stable and a small particle (circled) left the region of interest over just a few movie frames. The values for the velocity of the dissociation event (Figure 2D) have significant variability because of the frame rate (2 s/frame) at which the time lapse was acquired and the corresponding uncertainty in identifying the assemblage's location. Using current *in situ* STEM methodologies with these image acquisition settings, dynamic phenomena must occur on this 1–2 s time scale to be observed. The frame rate may be improved by using the conventional TEM mode;<sup>12</sup> however, contrast is challenging to interpret compared to Z-contrast STEM.

The experiments described here were highly controlled to minimize electron dose, which was maintained around  $1 \text{ e}^- \text{ \AA}^{-2} \text{ s}^{-1}$ . The electron beam interacts with water, producing an acidic environment in the liquid cell, as a function of dose rate.<sup>10,26,27</sup> At higher electron dose rates ( $\gg 1 \text{ e}^- \text{ \AA}^{-2} \text{ s}^{-1}$ ), goethite dissolved in the TEM liquid cell. New phases can arise through dissolution of the initial mineral material. We have observed the re-precipitation of new phases both with and without the  $C_{12}PO_4$  ligand (see Figure S3). The morphology of the re-precipitated material differed depending on whether the ligand was present. For goethite in water, dissolution was followed by precipitation of faceted iron hydroxide particles (see Figure S3b). Branching precipitates formed when  $C_{12}PO_4$  was present (see Figure S3a).

On the basis of these observations of organic–mineral interactions at the nanoscale, we speculate that the organic molecules bridge adjacent particles and stabilize larger assemblages, resulting in the observed 230% increase in assemblage size. Additionally, the side-to-side attachment is adopted in a manner independent of the addition of organic species, suggesting that the organic ligand does not play a large role in attachment of specific faces and the interaction between particles could be governed by a variety of forces, including hydrophobic or hydrodynamic forces. Additionally, *in situ* experiments did not reveal many reversible events.

While microassemblages are thought to contribute significantly to the most stable carbon pool in soils, their formation is poorly understood. There are different conceptual models. Some researchers postulate that fine mineral particles adhere to existing organic molecules,<sup>2</sup> while a second group suggests a mechanism by which polyvalent metals and organic ligands interact with mineral surfaces to stabilize assemblages.<sup>28,29</sup> The different roles of organic matter in these models of mineral assembly may be due to the variety of organic ligands. The choice of ligand and solution chemistry influences the role of the organic in either stabilizing assemblages or promoting aggregation. The phosphate ligand used here interacts strongly with iron oxide surfaces and may allow bridging between

mineral grains. In our results, no differences were observed in mineral orientation with or without an organic proxy (Figure 1D); however, the strong difference in assemblage size (Figure 1C) could potentially support the second conceptual model, as organic ligands can promote mineral aggregation.

The research presented here probes a simple system to provide a fundamental understanding of organic–mineral interactions from the molecular scale to the nanoscale. Via a combination of the dynamic information from *in situ* (S)TEM with that from the more statistically robust cryo-TEM, a more complete picture of organic–mineral systems can be realized. This approach can be extended beyond the simple model system shown here to more complex model systems (e.g., including electrolytes such as divalent cations), to different mineral classes, and to interrogation of natural organic matter.<sup>30,31</sup> For example, natural clay fractions from soil, with <2  $\mu\text{m}$  particles, are amenable to these methods. The challenge in imaging naturally occurring soil samples will be in differentiating the various mineral phases in a heterogeneous sample without damaging the sample with, e.g., high-dose diffraction experiments. As *in situ* techniques are applied more broadly, nanoscale characterization of even complex natural samples will be feasible. TEM visualization of submicrometer interactions provides nanoscale information for models and can be used to understand fundamental interactions that could guide experimental design at larger length scales. In this work, interactions between minerals and organics occurred on a time scale of 1 s. Slower, environmentally relevant processes on time scales of minutes, hours, months, or geologic periods can be observed by measuring samples at the appropriate times. However, we now know that adsorption of organic matter can occur at a rate much faster than 1 s. Dynamic TEM methodologies, for example, could push time scales into the unobserved nano- or picosecond time scales.<sup>32</sup> As a wider variety of relevant minerals and organic matter are explored at these fundamental length and time scales, there is potential to translate the behavior to other scales and relate these observations to the complex systems in soils.

## ■ ASSOCIATED CONTENT

### 📄 Supporting Information

The Supporting Information is available free of charge on the ACS Publications website at DOI: 10.1021/acs.estlett.7b00068.

Tables S1 and S2 and Figures S1–S3 showing DLS results, additional cryo-TEM measurements and a schematic of data analysis, and examples of electron beam effects (PDF)

Example association events (AVI)

Example dissociation events (AVI)

## ■ AUTHOR INFORMATION

### Corresponding Author

\*E-mail: Nik.Qafoku@pnnl.gov. Phone: 509-371-6089.

### ORCID

Ryan Hufschmid: 0000-0003-4557-8060

Jay W. Grate: 0000-0002-2163-8383

### Author Contributions

R.H. and C.J.N. contributed equally to this work and are listed in alphabetical order. R.H. and C.J.N. performed experiments. R.H., C.J.N., J.W.G., J.J.D.Y., N.D.B., and N.P.Q. wrote the manuscript and designed experiments.

## Notes

The authors declare no competing financial interest.

## ■ ACKNOWLEDGMENTS

This work was supported by the Chemical Imaging Initiative, a Laboratory Directed Research and Development program at Pacific Northwest National Laboratory (PNNL). PNNL is operated by Battelle for the Department of Energy (DOE) under Contract DE-AC05-76RL01830. A portion of the research was performed using the William R. Wiley Environmental Molecular Sciences Laboratory, a DOE national scientific user facility sponsored by the DOE's Office of Biological and Environmental Research and located at PNNL.

## ■ REFERENCES

- (1) Six, J.; Conant, R. T.; Paul, E. A.; Paustian, K. Stabilization Mechanisms of Soil Organic Matter: Implications for C-Saturation of Soils. *Plant Soil* **2002**, *241*, 155–176.
- (2) Tisdall, J. M.; Oades, J. M. Organic Matter and Water-Stable Aggregates in Soils. *J. Soil Sci.* **1982**, *33*, 141–163.
- (3) Schmidt, M. W. I.; Torn, M. S.; Abiven, S.; Dittmar, T.; Guggenberger, G.; Janssens, I. A.; Kleber, M.; Kögel-Knabner, I.; Lehmann, J.; Manning, D. A. C.; et al. Persistence of Soil Organic Matter as an Ecosystem Property. *Nature* **2011**, *478*, 49–56.
- (4) De Yoreo, J. J.; Sommerdijk, N. A. J. M. Investigating Materials Formation with Liquid-Phase and Cryogenic TEM. *Nat. Rev. Mater.* **2016**, *1*, 16035.
- (5) Kleber, M.; Eusterhues, K.; Keiluweit, M.; Mikutta, C.; Mikutta, R.; Nico, P. S. Mineral–Organic Associations: Formation, Properties, and Relevance in Soil Environments. *Adv. Agron.* **2015**, *130*, 1–140.
- (6) Taheri, M. L.; Stach, E. A.; Arslan, I.; Crozier, P. A.; Kabius, B. C.; LaGrange, T.; Minor, A. M.; Takeda, S.; Tanase, M.; Wagner, J. B.; et al. Current Status and Future Directions for *in Situ* Transmission Electron Microscopy. *Ultramicroscopy* **2016**, *170*, 86–95.
- (7) Liu, J.; Wang, Z.; Sheng, A.; Liu, F.; Qin, F.; Wang, Z. L. *In Situ* Observation of Hematite Nanoparticle Aggregates Using Liquid Cell Transmission Electron Microscopy. *Environ. Sci. Technol.* **2016**, *50*, 5606–5613.
- (8) de Jonge, N.; Ross, F. M. Electron Microscopy of Specimens in Liquid. *Nat. Nanotechnol.* **2011**, *6*, 695–704.
- (9) De Yoreo, J. J. *In-Situ* Liquid Phase TEM Observations of Nucleation and Growth Processes. *Prog. Cryst. Growth Charact. Mater.* **2016**, *62*, 69–88.
- (10) Woehl, T. J.; Evans, J. E.; Arslan, I.; Ristenpart, W. D.; Browning, N. D. Direct *In Situ* Determination of the Mechanisms Controlling Nanoparticle Nucleation and Growth. *ACS Nano* **2012**, *6*, 8599–8610.
- (11) Welch, D. A.; Woehl, T. J.; Park, C.; Faller, R.; Evans, J. E.; Browning, N. D. Understanding the Role of Solvation Forces on the Preferential Attachment of Nanoparticles in Liquid. *ACS Nano* **2016**, *10*, 181–187.
- (12) Li, D.; Nielsen, M. H.; Lee, J. R. I.; Frandsen, C.; Banfield, J. F.; De Yoreo, J. J. Direction-Specific Interactions Control Crystal Growth by Oriented Attachment. *Science* **2012**, *336*, 1014–1018.
- (13) Mehdi, B. L.; Qian, J.; Nasybulin, E.; Park, C.; Welch, D. A.; Faller, R.; Mehta, H.; Henderson, W. A.; Xu, W.; Wang, C. M.; et al. Observation and Quantification of Nanoscale Processes in Lithium Batteries by Operando Electrochemical (S)TEM. *Nano Lett.* **2015**, *15*, 2168–2173.
- (14) Hiemstra, T.; Van Riemsdijk, W. H. A Surface Structural Approach to Ion Adsorption: the Charge Distribution (CD) Model. *J. Colloid Interface Sci.* **1996**, *179* (2), 488–508.
- (15) Abellan, P.; Woehl, T. J.; Parent, L. R.; Browning, N. D.; Evans, J. E.; Arslan, I. Factors Influencing Quantitative Liquid (Scanning) Transmission Electron Microscopy. *Chem. Commun.* **2014**, *50* (38), 4873–4880.

- (16) Abellan, P.; Parent, L. R.; Al Hasan, N.; Park, C.; Arslan, I.; Karim, A. M.; Evans, J. E.; Browning, N. D. Gaining Control Over Radiolytic Synthesis of Uniform Sub-3-Nanometer Palladium Nanoparticles: Use of Aromatic Liquids in the Electron Microscope. *Langmuir* **2016**, *32*, 1468–1477.
- (17) Schneider, C. A.; Rasband, W. S.; Eliceiri, K. W. NIH Image to ImageJ: 25 Years of Image Analysis. *Nat. Methods* **2012**, *9*, 671–675.
- (18) Kleber, M.; Sollins, P.; Sutton, R. A Conceptual Model of Organo-Mineral Interactions in Soils: Self-Assembly of Organic Molecular Fragments Into Zonal Structures on Mineral Surfaces. *Biogeochemistry* **2007**, *85*, 9–24.
- (19) Krumina, L.; Kenney, J. P. L.; Loring, J. S.; Persson, P. Desorption Mechanisms of Phosphate From Ferrihydrite and Goethite Surfaces. *Chem. Geol.* **2016**, *427*, 54–64.
- (20) Turner, B. L., Frossard, E., Baldwin, D. S., Eds. *Organic Phosphorus in the Environment*; CABI: Wallingford, U.K., 2005.
- (21) Cagnasso, M.; Boero, V.; Franchini, M. A.; Chorover, J. ATR-FTIR Studies of Phospholipid Vesicle Interactions with A-FeOOH and A-Fe<sub>2</sub>O<sub>3</sub> Surfaces. *Colloids Surf., B* **2010**, *76*, 456–467.
- (22) Parikh, S. J.; Mukome, F. N. D.; Zhang, X. ATR-FTIR Spectroscopic Evidence for Biomolecular Phosphorus and Carboxyl Groups Facilitating Bacterial Adhesion to Iron Oxides. *Colloids Surf., B* **2014**, *119*, 38–46.
- (23) Persson, P.; Andersson, T.; Nelson, H.; Sjöberg, S.; Giesler, R.; Lövgren, L. Surface Complexes of Monomethyl Phosphate Stabilized by Hydrogen Bonding on Goethite (A-FeOOH) Nanoparticles. *J. Colloid Interface Sci.* **2012**, *386*, 350–358.
- (24) Lal, R. *Encyclopedia of Soil Science*, 3rd ed.; CRC Press: Boca Raton, FL, 2016.
- (25) Badaire, S.; Poulin, P.; Maugey, M.; Zakri, C. In situ Measurements of Nanotube Dimensions in Suspensions by Depolarized Dynamic Light Scattering. *Langmuir* **2004**, *20*, 10367–10370.
- (26) Schneider, N. M.; Norton, M. M.; Mendel, B. J.; Grogan, J. M.; Ross, F. M.; Bau, H. H. Electron-Water Interactions and Implications for Liquid Cell Electron Microscopy. *J. Phys. Chem. C* **2014**, *118*, 22373–22382.
- (27) Grogan, J. M.; Schneider, N. M.; Ross, F. M.; Bau, H. H. Bubble and Pattern Formation in Liquid Induced by an Electron Beam. *Nano Lett.* **2014**, *14*, 359–364.
- (28) Lehmann, J.; Kinyangi, J.; Solomon, D. Organic Matter Stabilization in Soil Microaggregates: Implications From Spatial Heterogeneity of Organic Carbon Contents and Carbon Forms. *Biogeochemistry* **2007**, *85*, 45–57.
- (29) Six, J.; Bossuyt, H.; Degryze, S.; Deneff, K. A History of Research on the Link Between (Micro)Aggregates, Soil Biota, and Soil Organic Matter Dynamics. *Soil Tillage Res.* **2004**, *79*, 7–31.
- (30) Vindedahl, A. M.; Stemig, M. S.; Arnold, W. A.; Penn, R. L. Character of Humic Substances as a Predictor for Goethite Nanoparticle Reactivity and Aggregation. *Environ. Sci. Technol.* **2016**, *50*, 1200–1208.
- (31) Vindedahl, A. M.; Arnold, W. A.; Lee Penn, R. Impact of Pahokee Peat Humic Acid and Buffer Identity on Goethite Aggregation and Reactivity. *Environ. Sci.: Nano* **2015**, *2*, 509–517.
- (32) Browning, N. D.; Bonds, M. A.; Campbell, G. H.; Evans, J. E.; LaGrange, T.; Jungjohann, K. L.; Masiel, D. J.; McKeown, J.; Mehraeen, S.; Reed, B. W.; Santala, M. Recent developments in dynamic transmission electron microscopy. *Curr. Opin. Solid State Mater. Sci.* **2012**, *16*, 23–30.